FUNCTION™ american physiological society

FUNCTION, 2022, 3(3): zqac013

https://doi.org/10.1093/function/zqac013
Advance Access Publication Date: 17 March 2022
Original Research

RESEARCH ARTICLE

ADAM17 Mediates Proteolytic Maturation of Voltage-Gated Calcium Channel Auxiliary $\alpha_2\delta$ Subunits, and Enables Calcium Current Enhancement

Ivan Kadurin[1,†], Shehrazade Dahimene[1], Karen M. Page[1], Joseph I. J. Ellaway[1], Kanchan Chaggar[1], Linda Troeberg[2], Hideaki Nagase[3], Annette C. Dolphin[1,*]

[1]Department of Neuroscience, Physiology and Pharmacology, University College London, London WC1E 6BT, UK, [2]Norwich Medical School, University of East Anglia, Norwich NR4 7UQ, UK and [3]Kennedy Institute of Rheumatology, University of Oxford, Oxford OX3 7FY, UK

*Address correspondence to A. C. D. (e-mail: a.dolphin@ucl.ac.uk)

†Present address: School of Biological and Behavioural Sciences, Queen Mary University of London; i.kadurin@qmul.ac.uk

Abstract

The auxiliary $\alpha_2\delta$ subunits of voltage-gated calcium (Ca_V) channels are key to augmenting expression and function of Ca_V1 and Ca_V2 channels, and are also important drug targets in several therapeutic areas, including neuropathic pain. The $\alpha_2\delta$ proteins are translated as preproteins encoding both α_2 and δ, and post-translationally proteolyzed into α_2 and δ subunits, which remain associated as a complex. In this study, we have identified ADAM17 as a key protease involved in proteolytic processing of pro-$\alpha_2\delta$-1 and $\alpha_2\delta$-3 subunits. We provide three lines of evidence: First, proteolytic cleavage is inhibited by chemical inhibitors of particular metalloproteases, including ADAM17. Second, proteolytic cleavage of both $\alpha_2\delta$-1 and $\alpha_2\delta$-3 is markedly reduced in cell lines by knockout of *ADAM17* but not *ADAM10*. Third, proteolytic cleavage is reduced by the N-terminal active domain of TIMP-3 (N-TIMP-3), which selectively inhibits ADAM17. We have found previously that proteolytic cleavage into mature $\alpha_2\delta$ is essential for the enhancement of Ca_V function, and in agreement, knockout of ADAM17 inhibited the ability of $\alpha_2\delta$-1 to enhance both $Ca_V2.2$ and $Ca_V1.2$ calcium currents. Finally, our data also indicate that the main site of proteolytic cleavage of $\alpha_2\delta$-1 is the Golgi apparatus, although cleavage may also occur at the plasma membrane. Thus, our study identifies ADAM17 as a key protease required for proteolytic maturation of $\alpha_2\delta$-1 and $\alpha_2\delta$-3, and thus a potential drug target in neuropathic pain.

Submitted: 7 February 2022; **Revised:** 9 March 2022; **Accepted:** 10 March 2022

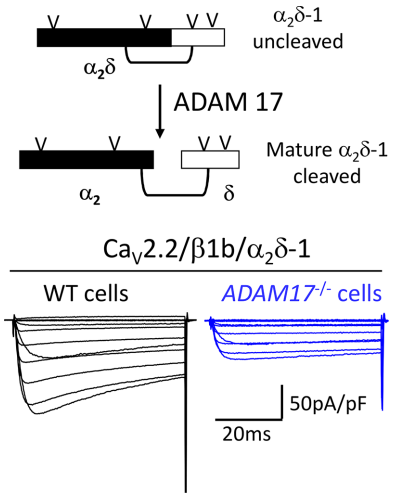

Key words: calcium channel; $\alpha_2\delta$ subunit; matrix metalloprotease; ADAM17; trafficking; calcium currents

Introduction

Voltage-gated calcium (Ca_V) channels are essential for multiple physiological functions including neurotransmitter release and muscle contraction, and are also important drug targets in several therapeutic areas, including chronic pain.[1,2] There are three subtypes of Ca_V channel pore-forming α_1 subunit (Ca_V1, 2, and 3), of which Ca_V1 and 2 are associated with auxiliary β and $\alpha_2\delta$ subunits,[3–6] which are both important for their function (for review see[7]).

The $\alpha_2\delta$ subunits are extracellular proteins that undergo complex post-translational modifications (Figure 1A). A single gene encodes each $\alpha_2\delta$ preprotein, which is then subject to several processing steps, including glycosyl-phosphatidylinositol (GPI)-anchoring,[8] extensive glycosylation, and proteolytic processing into disulfide-linked α_2 and δ.[9,10] The cryoelectron microscopic structure of the skeletal muscle $Ca_V1.1$ complex[11] shows interaction of $\alpha_2\delta$-1 with several extracellular loops of the α_1 subunit, including a key residue in the first extracellular loop of Domain I, which interacts with the von Willebrand factor (VWA) domain of $\alpha_2\delta$-1.

The $\alpha_2\delta$ subunits generally increase Ca^{2+} currents produced by $Ca_V\alpha_1/\beta$ combinations, by a mechanism that is not yet completely understood.[12,13] We have shown that $\alpha_2\delta$-1 increases the density of $Ca_V2.2$ channels inserted into the plasma membrane,[14–16] and produces a large increase in calcium channel currents.[17–19] For $Ca_V2.2$, the interaction of Domain I extracellular loop 1 with the $\alpha_2\delta$ VWA domain is absolutely essential for its effect on trafficking and function.[15,17]

Proteolytic processing is important for the maturation of many proteins (for example,[20,21]), as well as being essential for protein degradation.[22] In an extensive study, we have found that proteolytic maturation of $\alpha_2\delta$ subunits is an essential step for activation of plasma membrane calcium channels. By replacing the proteolytic cleavage site in $\alpha_2\delta$ with an artificial site (α_2(3C)δ), we found that uncleaved $\alpha_2\delta$-1 inhibits native calcium currents in DRG neurons.[13] Furthermore, uncleaved $\alpha_2\delta$-1 inhibits presynaptic Ca^{2+} entry and vesicular release in hippocampal neurons.[13,23] We also showed that in non-neuronal cells the effect of $\alpha_2\delta$ on Ca_V channel activation can be separated from its trafficking role, in that uncleaved α_2(3C)δ-1 and α_2(3C)δ-3 can traffic $Ca_V2.2$ channels to the plasma membrane, but these uncleaved constructs do not enhance $Ca_V2.2$ currents, unless proteolytic cleavage is artificially induced.[13] Thus, we proposed that proteolytic processing of $\alpha_2\delta$ subunits represents an activation step for calcium channel function, and pro-$\alpha_2\delta$ subunits maintain the channels in a state of low activation.

Upregulation of $\alpha_2\delta$-1 protein is of importance in the development of neuropathic pain,[24–27] and $\alpha_2\delta$-1 is also the drug target for gabapentinoid drugs used in neuropathic pain.[28,29] These drugs inhibit calcium channel trafficking when applied chronically.[14,18] In the present study, we have examined the nature of the enzyme(s) involved in proteolytic cleavage of $\alpha_2\delta$ subunits, since inhibition of its proteolytic cleavage could represent a novel point of therapeutic intervention.

Methods

Molecular Biology

The following cDNAs were used: $Ca_V2.2$ (rabbit, D14157), $Ca_V2.2$-HA,[14] GFP_$Ca_V2.2$-HA,[30] $Ca_V1.2$ (rat; M67515.1), β1b (rat, X61394),[31] β3 (rat; M88751), $\alpha_2\delta$-1 (rat, M86621),[32] HA-$\alpha_2\delta$-1,[33] $\alpha_2\delta$-3 (AJ010949), HA- $\alpha_2\delta$-3,[13] mCherry,[34] mut2-GFP,[35] Arf(Q71L)-CFP (Addgene plasmid # 128149),[36] and CFP replaced with mCherry. The cDNAs were in the pcDNA3 vector for expression in tsA-201 and HEK293 cells. CD8 cDNA[37] was included as a transfection marker where stated.

Antibodies and Other Materials

Antibodies (Abs) used were: Anti-$\alpha_2\delta$-1 Ab (mouse monoclonal, Sigma-Aldrich), anti-$\alpha_2\delta$-3 and anti-δ-3 Ab,[8] anti-HA Ab (rat monoclonal, Roche), anti-GAPDH Ab (mouse monoclonal, Ambion), anti-FLAG Ab (rabbit polyclonal; Sigma), anti-PDI (mouse monoclonal, Ambion), anti-g97 (rabbit polyclonal; Abcam), and anti-flotillin Ab (monoclonal, BD Biosciences). For immunoblotting, secondary Abs (1:2000) were anti-rabbit–Horseradish Peroxidase (HRP), and anti-mouse HRP (Biorad). For immunocytochemistry, anti-rat-Alexa Fluor 594 was used at 1/500 (ThermoFisher).

The metalloprotease inhibitors GM6001 (BML-EI300, Enzo Life Sciences), SB-3CT (BMEI325, Enzo Life Sciences), and MMP-13 inhibitor (BML-EI302, Enzo Life Sciences) were dissolved in DMSO (or water for MMP-13 inhibitor) and used at the concentrations stated. N-TIMP-3 protein (expressed in *Escherichia coli* as

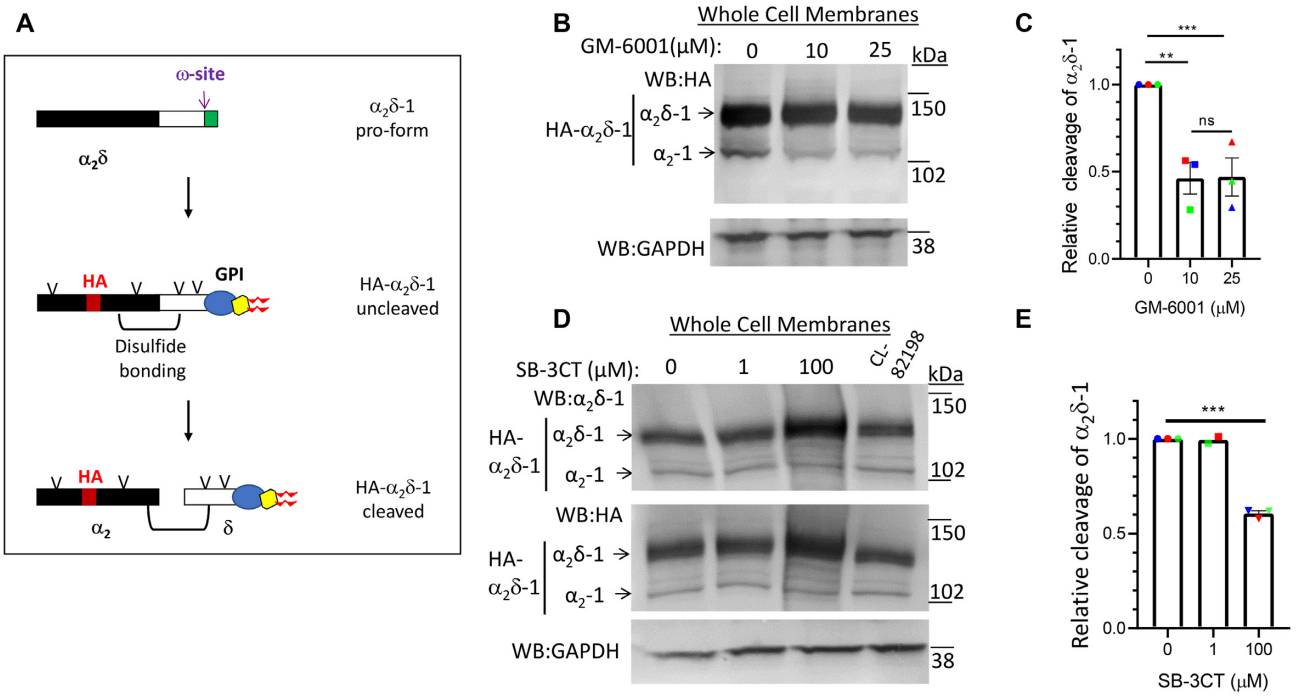

Figure 1. Effect of chemical inhibitors of ADAMs and MMPs on $\alpha_2\delta$-1 proteolytic cleavage. (A) Diagram of post-translational processing of $\alpha_2\delta$ proteins, including glycosylation (V), GPI anchoring, and proteolytic cleavage. It also shows the approximate position of inserted HA tag (red) and disulfide bonding between α_2 (black) and δ (white). (B) Effect of GM-6001 (0, 10, and 25 μM; lanes 1–3, respectively) on cleavage in whole cell membranes of HA-$\alpha_2\delta$-1 expressed in tsA-201 cells (upper panel: HA immunoblot), deglycosylated with PNGase-F to allow resolution between pro-$\alpha_2\delta$-1 (upper band) and the cleaved form, α_2–1 (lower band). The absolute % cleavage was 12.8 ± 2.0% in control conditions. Lower panel, loading control: Endogenous GAPDH. (C) Quantification of the effect of 10 μM (squares) and 25 μM (triangles) GM-6001 on relative cleavage of $\alpha_2\delta$-1 (normalized to that under control conditions (circles)). Data are mean ± SEM and individual data in three separate experiments, including that in (B), denoted by red, green, and blue symbols. Statistical differences determined using 1-way ANOVA and Tukey post hoc test; ** $P = .0084$; *** $P = .0090$. (D) Effect of SB-3CT (0, 1, and 100 μM; lanes 1–3, respectively) and CL-82198 (60 μM; lane 4) on cleavage in whole cell membranes of HA-$\alpha_2\delta$-1 expressed in tsA-201 cells. Top panel: $\alpha_2\delta$-1 immunoblot and middle panel: HA immunoblot, both deglycosylated to allow resolution between pro-$\alpha_2\delta$-1 (upper band) and the cleaved form, α_2–1 (lower band). Bottom panel: Loading control endogenous GAPDH. The absolute % cleavage was 11.2 ± 1.0% in control conditions. (E) Quantification of the effect of 1 and 100 μM SB-3CT on relative cleavage of $\alpha_2\delta$-1, measured from HA immunoblots (normalized to that under control conditions). Data are mean ± SEM and individual data in three separate experiments, including that in (D), denoted by red, green, and blue symbols). Statistical differences determined using 1-way ANOVA and Tukey post hoc test; *** $P < .0001$.

previously described,[38]) or control samples in the absence of N-TIMP-3, were preincubated with heparin (200 μg/ml) for an hour at 37°C before adding to the cells.

Cell Lines and Cell Culture

The cell lines were plated onto cell culture flasks or coverslips, coated with poly-L-lysine, and cultured in a 5% CO_2 incubator at 37°C. The tsA-201 cells (European Collection of Cell Cultures (ECACC), female sex) were cultured in Dulbecco's modified Eagle's medium (DMEM) supplemented with 10% foetal bovine serum (FBS), 1 unit/mL penicillin, 1 μg/mL streptomycin, and 1% GlutaMAX (Life Technologies, Waltham, MA). When protease inhibitors were used, they were applied 12 h after transfection by replacing the medium with serum-free DMEM F12 (supplemented with 1 unit/mL penicillin, 1 μg/mL streptomycin, and 1% GlutaMAX) containing the inhibitors, as indicated. The cells were incubated in culture for 24 h before harvesting. The production and verification of the CRISPR WT and knockout HEK293 ADAM17$^{-/-}$ and ADAM10$^{-/-}$ cells is described previously.[39] The SH-SY5Y human neuroblastoma cell line (ECACC # 94030304; female sex)[40] stably expressing HA-$\alpha_2\delta$-3 was generated in the laboratory by standard techniques, described previously.[41]

Cell Line Transfection

For electrophysiological studies, CRISPR WT and knockout HEK293 cells were transfected with $Ca_V2.2$-HA or $Ca_V1.2$ together with $\alpha_2\delta$-1 and β1b or β3 (all in vector pcDNA3) in a ratio 3:2:2. The transfection reagent used was PolyJet (Tebu-bio Ltd), used in a ratio of 3:1 to DNA mix. Culture medium was changed 12 h after transfection and cells were incubated at 37°C for a further 42 h. CD8 was used as transfection marker.

For cell surface biotinylation and other biochemical experiments, tsA-201 cells were transfected using Fugene6 (Promega) according to the manufacturer's protocol. CRISPR WT and knockout HEK293cells were transfected with PolyJet as above, and incubated at 37°C for 48 h.

Preparation of WCL, Deglycosylation, Cell Surface Biotinylation, and Immunoblotting

Cell surface biotinylation experiments were carried out on tsA-201 or HEK293 CRISPR WT and knockout cells expressing the cDNAs described. At 48 h after transfection, cells were rinsed with phosphate-buffered saline (PBS) and then incubated for 30 min at room temperature (RT) with 0.5 mg/mL Premium Grade EZ-link Sulfo-NHS-LC-Biotin (Thermo Scientific) in PBS. The reaction was quenched by removing the biotin solution and

replacing with PBS containing 200 mM glycine for 2 min at RT. The cells were rinsed with PBS before being resuspended in PBS containing 1% Igepal; 0.1% SDS, and protease inhibitors (PI, cOmplete, Sigma-Aldrich), pH 7.4, for 30 min on ice to allow cell lysis. WCL were then cleared by centrifugation at 13 000 × *g* and assayed for total protein (Bradford assay, Biorad). Biotinylated lysates were equalized to between 0.5 and 1 mg/mL total protein concentration; 0.5 mg of these biotinylated lysates were adjusted to 500 μL and applied to 40 μL prewashed streptavidin–agarose beads (Thermo Scientific) and rotated overnight at 4°C. The streptavidin beads were then washed 3 times with PBS containing 0.1% Igepal, and resuspended in Peptide N-glycosidase (PNG)-ase-F buffer (PBS, pH 7.4, supplemented with 75 mM β-mercaptoethanol, 1% Igepal, 0.1% SDS, and PI) and deglycosylated for 3 h at 37°C with 1 unit of PNGase-F (Roche Applied Science) added per 10 μL volume. When Endo-H was used, a sample of washed beads was removed (before PNGase-F was added), denatured at 99°C for 10 min and treated with Endo-H (New England Biosciences) for 1 h at 37°C. Samples were then resuspended in an equal volume of 2x Laemmli buffer,[8] supplemented with dithiothreitol (DTT) to a final concentration of 100 mM, and heated for 10 min at 60°C to elute the precipitated protein. Aliquots of cleared WCL, corresponding to 20–40 μg total protein were deglycosylated in parallel, as described above.[13] The samples were then resuspended in an equal volume of 2x Laemmli buffer (with 100 mM DTT), followed by 10 min incubation at 60°C before loading on SDS-polyacrylamide gel electrophoresis (PAGE). The samples were then resolved by SDS-PAGE on 3%–8% Tris-Acetate gels (Thermo Fisher Scientific) and transferred to polyvinylidene fluoride (PVDF) membranes (Biorad). The membranes were blocked with 5% bovine serum albumin (BSA), 0.5% Igepal in Tris-buffered saline (TBS) for 30 min at RT and then incubated overnight at 4°C with the relevant primary Ab. After washing in TBS containing 0.5% Igepal, membranes were incubated with the appropriate secondary Ab for 1 h at RT. The signal was obtained by HRP reaction with fluorescent product (ECL 2; Thermo Scientific) and membranes were scanned on a Typhoon 9410 phosphorimager (GE Healthcare).

Preparation of Whole Cell Membrane Fraction and of Detergent Resistant Membranes (DRMs)

Cell pellets of a confluent T-75 flask were resuspended in 1 mL of ice-cold buffer containing 10 mM NaCl, 10 mM HEPES, pH 7.4, and PI. Cells were lysed by 10 passages through a 25-gauge syringe, followed by three 10-s rounds of sonication. Cell debris was removed by centrifugation (1000 × *g*, for 10 min at 4°C), and the resultant supernatants were recentrifuged (60 000 × *g*, for 60 min at 4°C) to pellet membranes. The whole cell membrane fraction was resuspended in 50 μL of PNGase-F buffer and deglycosylated for 3 h at 37°C with 1 unit of PNGase-F added per 10 μL volume.

The protocol for preparation of DRMs was similar to that described previously.[8,33] All steps were performed on ice. Confluent tsA-201 cells from two 175 cm^2 flasks were taken up in Mes-buffered saline (MBS, 25 mM Mes, pH 6.5, 150 mM NaCl, and PI) containing 1% (v/v) Triton X-100 (TX-100; Thermo Scientific), and left on ice for 1 h. An equal volume of 90% (w/v) sucrose in MBS was then added to a final concentration of 45% sucrose. The sample was transferred to a 13-mL ultracentrifuge tube and overlaid with 10 mL of discontinuous sucrose gradient, consisting of 35% (w/v) sucrose in MBS (5 mL) and 5% (w/v) sucrose in MBS (5 mL). The sucrose gradients were ultracentrifuged at 140 000 × g_{avg} (Beckman SW40 rotor) for 18 h at 4°C. 1 mL fractions were subsequently harvested from the top to the bottom of the tube and aliquots of 10 μL from each fraction were analysed by SDS-PAGE and western blotting to obtain DRM profiles. When necessary, DRMs (combined peak fractions identified by presence of flotillin-1) from the gradient were washed free of sucrose by dilution into 25 volumes of cold PBS (pH 7.4) and pelleted by ultracentrifugation at 150 000 × *g* (Beckman Ti 70 rotor) for 1 h at 4°C. TX-100-insoluble protein was resuspended in PNGase-F buffer and deglycosylated for 3 h at 37°C with 1 unit of PNGase-F added per 10 μL volume. The samples were then resuspended in Laemmli buffer (1x final concentration, with 100 mM DTT) followed by 10 min incubation at 60°C before loading on SDS-PAGE.

Subcellular Fractionation of SH-SY5Y Cell Line Stably Expressing HA-$\alpha_2\delta$-3 Subunits

The subcellular fractionation was performed in a continuous iodixanol gradient within the range 0%–25% (w/v) iodixanol to resolve the major membrane compartments of the ER, Golgi membranes from a postnuclear supernatant prepared from a cultured cell homogenate, as described previously.[42] Briefly, two T-175 flasks of SH-SY5Y cells (~ 70% confluent) stably expressing HA-$\alpha_2\delta$-3 were washed with PBS, and suspended in 3 mL of Homogenization Medium (HM, 0.25 M sucrose, 1 mM EDTA, 10 mM Tris, pH 7.4; supplemented with PI). Cell pellets were disrupted using a 25-gauge syringe (5 x passes), and centrifuged at 1000 × *g* for 10 min. A 25% (w/v) iodixanol solution was prepared by mixing equal volumes of HM and Working Solution (5 vol of OptiPrep + 1 vol of diluent (0.25 M sucrose, 6 mM EDTA, 60 mM Tris, pH 7.4); supplemented with PI). A 10-mL gradient was prepared in Beckman SW40 rotor tubes, using equal volumes of HM and the 25% iodixanol solution using a two-chamber gradient maker. A volume of 1 mL of the supernatants from the 1000 × *g* centrifugation were laid on top of the gradient and centrifuged at 200 000 × *g* (Beckman SW40 rotor) for 4 h. Fractions (0.75 mL) were collected from the top. Aliquots of each fraction were supplemented with Triton X100 to 0.5%, SDS to 0.1%, β-mercaptoethanol to 75 mM, and deglycosylated with PNGase-F as described above. 5x Laemmli buffer was then added (1x final concentration, with 100 mM DTT) followed by 10 min incubation at 60°C before loading on SDS-PAGE.

Electrophysiology

Calcium channel currents in transfected HEK293 CRISPR WT and knockout cells were investigated by whole cell patch-clamp recording, essentially as described previously.[43] The patch pipette solution contained in mM: Cs-aspartate, 140; EGTA, 5; $MgCl_2$, 2; $CaCl_2$, 0.1; K_2ATP, 2; Hepes, 20; and pH 7.2, 310 mOsm with sucrose. The external solution for recording Ba^{2+} currents contained in mM: tetraethylammonium (TEA) Br, 160; KCl, 3; $NaHCO_3$, 1; $MgCl_2$, 1; Hepes, 10; glucose, 4; $BaCl_2$, (1 for $Ca_V2.2$ currents and 5 for $Ca_V1.2$ currents); and pH 7.4, 320 mosM with sucrose. An Axopatch 1D or Axon 200B amplifier was used, and whole cell voltage-clamp recordings were sampled at 10 kHz frequency, filtered at 2 kHz and digitized at 1 kHz. A total of 70%–80% series resistance compensation was applied and all recorded currents were leak subtracted using P/8 protocol. Membrane potential was held at −80 mV. Analysis was performed using Pclamp 9 (Molecular Devices) and Origin 2017 (Microcal Origin, Northampton, MA). Current–voltage (*I*–*V*) relationships were fit by a modified Boltzmann equation as follows: $I = G_{max}*(V\text{-}V_{rev})/(1 + exp(-(V\text{-}V_{50,\,act})/k))$, where *I* is the current

density (in pA/pF), G_{max} is the maximum conductance (in nS/pF), V_{rev} is the apparent reversal potential, $V_{50,\,act}$ is the midpoint voltage for current activation, and k is the slope factor.

Immunocytochemistry, Imaging, and Analysis

Immunocytochemistry was carried out on HEK293 CRISPR WT and knockout cells expressing GFP_Ca_V2.2-HA together with $\alpha_2\delta$-1 and β1b. After transfection, cells were incubated for 48 h before being fixed with 4% paraformaldehyde (PFA) in PBS, pH 7.4 at RT for 5 min. Blocking was performed for 30 min at RT in PBS containing 20% goat serum and 5% BSA. An anti-HA Ab (rat monoclonal) was applied (100 ng/mL dilution in PBS with 10% goat serum and 2.5% BSA) for 1 h at RT to the nonpermeabilized cells. Cells were then incubated with an anti-rat Alexa Fluor 594 (1:500 dilution in PBS, containing 2.5% BSA and 10% goat serum) at RT for 1 h. The coverslips were mounted onto glass slides using VECTASHIELD® mounting medium (Vector Laboratories, Peterborough, UK).

Imaging was performed on Zeiss LSM 780 confocal microscope, at fixed microscope settings for all experimental conditions of each experiment. Images of HEK293 CRISPR WT and knockout cells were obtained using a 63x oil objective at a resolution of 1024 × 1024 pixels and an optical section of 0.5 μm. After choosing a region of interest containing transfected cells, the 3 × 3 tile function of the microscope allowed imaging of a larger area selected without bias. Every cell identified as transfected was included in the measurements, to ensure lack of bias.

Images of HEK293 CRISPR WT and knockout cells were analyzed using ImageJ (imagej.net). Cell surface signal was quantified using the freehand line (3 pixels) to trace the membrane region stained by anti-HA Ab. The total level of Ca_V2.2 corresponding to the GFP signal was measured using the freehand selection tool, excluding the nucleus. The value of the mean pixel intensity in different channels was measured separately and background was subtracted by measuring the intensity of an imaged area without transfected cells. The ratio of cell surface to total Ca_V2.2 (HA/GFP) was then calculated for each cell. The data are shown as mean ± SEM and single data points (for six independent transfections, in which all conditions were examined in parallel).

Quantification and Statistical Analysis

Data were analyzed with GraphPad Prism 8 (GraphPad software, San Diego, CA) or Origin-Pro 2017 (OriginLab Corporation, Northampton, MA). All data are shown as mean ± SEM; "n" refers to number of experiments, unless indicated otherwise, and is given in the figure legends, together with details of statistical tests used. Experiments where representative data are shown were repeated at least three times, as stated. Graphpad Prism 8 was used for statistical analysis. Statistical significance between two groups was assessed by Student's t-test, as stated. One-way or two-way ANOVA and the stated post hoc analysis was used for comparison of means between three or more groups.

Results

Sequence of Cleavage Site in $\alpha_2\delta$-1 Predicts Metalloproteases and ADAMs as Candidate Proteases

The proteolytic cleavage site in $\alpha_2\delta$-1 has been identified to be between A and V in the sequence LEA∼VEME[9,44] (A945 and V946 in the rat sequence used here, Figure 1A), and we have shown that mutation of this site prevents the cleavage of $\alpha_2\delta$-1 and abolishes the ability of $\alpha_2\delta$-1 to increase calcium channel currents.[13] Initial scrutiny of this sequence suggested a role for matrix metalloprotease (MMP) enzymes, specifically A Disintegrin and Metalloprotease (ADAM)10 or ADAM17/Tumor necrosis factor (TNF)-α converting enzyme (TACE). Although there are no absolute consensus motifs for proteolytic processing by these enzymes, there are preferred residues in the vicinity of the cleavage site[45]; for example the site in a well-established ADAM17 substrate Notch is IEA∼VKSE.[46] However, it should be noted that the proposed cleavage sites in $\alpha_2\delta$-2 and $\alpha_2\delta$-3 do not have similar primary sequences to that in $\alpha_2\delta$-1.[13]

We have found previously that proteolytic cleavage of $\alpha_2\delta$ subunits is incomplete when it is expressed in cell lines, possibly attributable to saturation of the endogenous protease(s) required for cleavage.[8,13,33] However, the degree of cleavage of $\alpha_2\delta$-1 is increased at the plasma membrane and in detergent resistant membranes (DRMs), also called lipid rafts, to about 60%,[33] and we found the same result in the present study. Importantly, the increased cleavage of $\alpha_2\delta$-1 observed at the cell surface and in DRMs is not likely to be a result of differential trafficking of cleaved relative to uncleaved $\alpha_2\delta$-1, since mutant uncleavable $\alpha_2\delta$-1 is still able to reach the plasma membrane to the same extent as WT $\alpha_2\delta$-1.[13]

Chemical Inhibitors of MMPs/ADAMs Reduce Proteolytic Cleavage of $\alpha_2\delta$s

In order to examine whether MMPs or ADAMs were involved in $\alpha_2\delta$-1 proteolytic cleavage, we first used a broad-spectrum hydroxamate metalloprotease inhibitor GM-6001, which inhibits both MMPs and ADAMs.[47] GM-6001 produced more than 50% inhibition of $\alpha_2\delta$-1 cleavage in whole cell membranes, when applied to tsA-201 cells at both 10 and 25 μM for 24 h (Figure 1B and C). The more selective inhibitor, SB-3CT, produced no inhibition at 1 μM, which is below the K_i for ADAM17 (∼4 μM),[48] but resulted in about 40% reduction at 100 μM ($P < .0001$, Figure 1D and E). In contrast, the MMP 13 inhibitor CL-82198 (60 μM) produced no inhibition of $\alpha_2\delta$-1 cleavage (Figure 1D).

Reduced Proteolytic Cleavage of $\alpha_2\delta$-1 in *ADAM17*$^{-/-}$ But Not *ADAM10*$^{-/-}$ Cell Lines

The activation of endogenous MMPs and ADAMs often involves a complex sequential proteolytic cascade[49]; for example, endogenous ADAM17 is activated by proteolytic cleavage with both furin and meprin β.[50] For this and other reasons, overexpression of candidate proteases is often not a successful experimental route to identification of their role in biochemical pathways (see for example[51]). Thus, in order to examine the potential involvement of ADAM17 in cleavage of $\alpha_2\delta$-1, we turned to HEK293 cell lines in which *ADAM10*, *ADAM17*, or both protease genes were knocked out by CRISPR/Cas9 methodology, in comparison to the corresponding CRISPR wild type (WT) cells.[39]

In initial experiments, we observed a marked reduction in proteolytic cleavage of $\alpha_2\delta$-1 in whole cell lysates (WCL) of CRISPR *ADAM10*$^{-/-}$/*ADAM17*$^{-/-}$ double knockout cells, compared to CRISPR WT HEK293 cells (Figure 2A). This was also clearly observed in the cell surface biotinylated fraction of these cells, in which greater basal cleavage is seen (Figure 2B). There

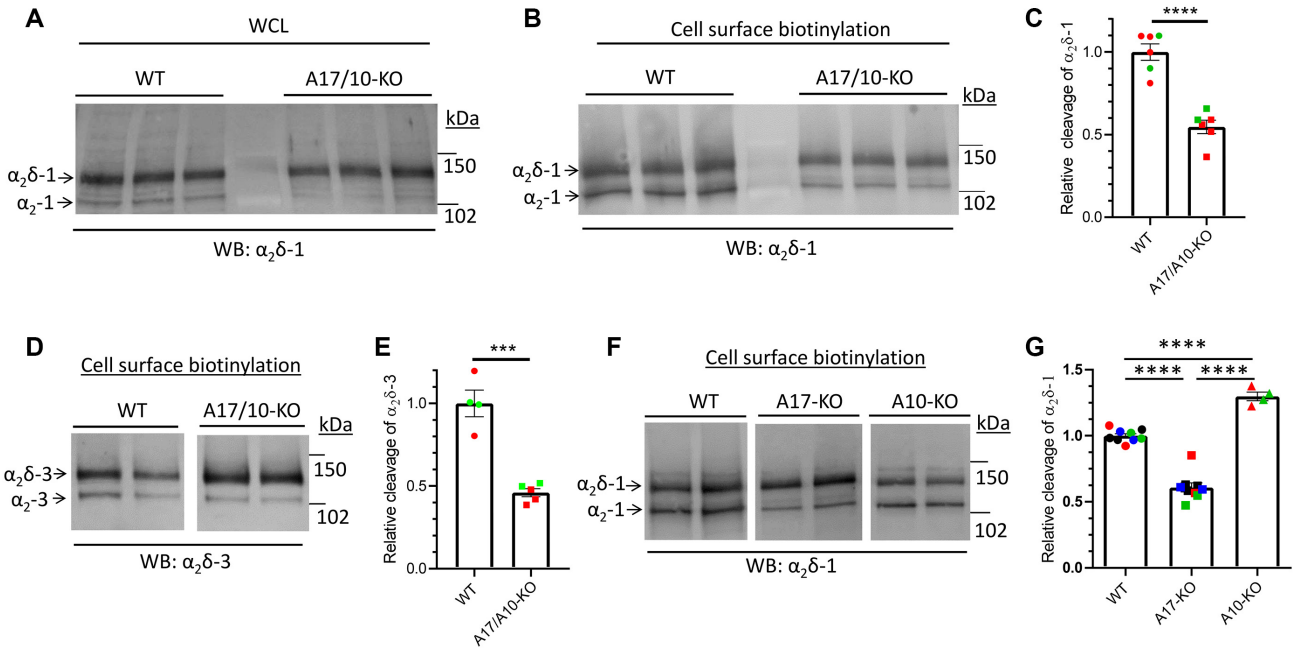

Figure 2. Cleavage of $\alpha_2\delta$-1 and $\alpha_2\delta$-3 is reduced in CRISPR *ADAM17*$^{-/-}$/*ADAM10*$^{-/-}$ and *ADAM17*$^{-/-}$ compared to CRISPR WT cells. (A) Effect of expression of $\alpha_2\delta$-1 in CRISPR WT (lanes 1–3) compared to CRISPR *ADAM17*$^{-/-}$/*ADAM10*$^{-/-}$ (A17/10-KO) HEK293 cells (lanes 4–6) on cleavage of HA-$\alpha_2\delta$-1 (α_2–1 immunoblot) in WCL, deglycosylated to allow resolution between pro-$\alpha_2\delta$-1 (upper band) and the cleaved form, α_2–1 (lower band). The absolute % cleavage was 21.2 ± 1.4% in CRISPR WT cells and 11.05 ± 1.2% in *ADAM17*$^{-/-}$/*ADAM10*$^{-/-}$ cells (n = 4 experiments). (B) Effect of expression of $\alpha_2\delta$-1 in CRISPR WT (lanes 1–3) compared to *ADAM17*$^{-/-}$/*ADAM10*$^{-/-}$ (A17/10-KO) HEK293 cells (lanes 4–6) on cleavage of HA-$\alpha_2\delta$-1 (α_2–1 immunoblot) in deglycosylated cell surface biotinylated fractions. The absolute % cleavage was 37.4 ± 2.4% in CRISPR WT cells (n = 6 experiments). (C) Quantification of the effect of expression in *ADAM17*$^{-/-}$/*ADAM10*$^{-/-}$ cells on relative cleavage of $\alpha_2\delta$-1 in cell surface biotinylated fraction, normalized to that in CRISPR WT cells. Data are mean ± SEM and individual data from six separate experiments, performed on two different transfections (red and green symbols). Statistical difference determined using Student's t-test; P = .0004. (D) Effect of expression of $\alpha_2\delta$-3 in CRISPR WT (lanes 1 and 2) compared to *ADAM17*$^{-/-}$/*ADAM10*$^{-/-}$ HEK293 cells (lanes 3 and 4) on cleavage of HA-$\alpha_2\delta$-3 in cell surface biotinylated fraction (α_2–3 immunoblot), deglycosylated to allow resolution between pro-$\alpha_2\delta$-3 (upper band) and the cleaved form, α_2–3 (lower band). The absolute % cleavage was 23.3 ± 2.5% in CRISPR WT cells (n = 4). (E) Quantification of the effect of *ADAM17*$^{-/-}$/*ADAM10*$^{-/-}$ on relative cleavage of $\alpha_2\delta$-3 in cell surface biotinylated fraction (normalized to that in CRISPR WT cells). Data are mean ± SEM and individual data in 4–5 separate experiments, performed on two separate transfections (red and green symbols). Statistical difference determined using Student's t-test; ***P = .0002. (F) Effect of expression of $\alpha_2\delta$-1 in CRISPR WT (lanes 1 and 2) compared to *ADAM17*$^{-/-}$ (lanes 3 and 4) and *ADAM10*$^{-/-}$ (lanes 5 and 6) HEK293 cells on cleavage of HA-$\alpha_2\delta$-1 (α_2–1 immunoblot) in cell surface biotinylated fractions, deglycosylated to allow resolution between pro-$\alpha_2\delta$-1 (upper band) and the cleaved form, α_2–1 (lower band). The absolute % cleavage was 44.5 ± 2.7% in CRISPR WT cells (n = 9). (G) Quantification of the effect of expression in *ADAM10*$^{-/-}$ and *ADAM17*$^{-/-}$ cells on relative cleavage of $\alpha_2\delta$-1 in cell surface biotinylated fraction, normalized to that in CRISPR WT cells. Data are mean ± SEM and individual data for nine separate experiments from four different transfections (all including WT and *ADAM17*$^{-/-}$ cells, and four also including *ADAM10*$^{-/-}$cells; colored symbols refer to different experiments). Statistical differences determined using one-way ANOVA and Tukey's multiple comparison test; ****P < .0001.

was a 45.3% reduction in proteolytic cleavage of $\alpha_2\delta$-1 at the cell surface of *ADAM10*$^{-/-}$/*ADAM17*$^{-/-}$ cells (P = .0004; Figure 2C). Furthermore, similar results were obtained in DRMs from *ADAM10*$^{-/-}$/*ADAM17*$^{-/-}$ cells, (32% reduction in $\alpha_2\delta$-1 cleavage; P = .049; Figure S1A and B). There was no change in the distribution of $\alpha_2\delta$-1 in DRMs from *ADAM10*$^{-/-}$/*ADAM17*$^{-/-}$ cells (Figure S1C).

Although the identified $\alpha_2\delta$-3 proteolytic cleavage motif has a primary sequence that is different from that of $\alpha_2\delta$-1,[13] the ADAM proteases support a wide divergence of cleavage motifs (see for example[52]). We, therefore, performed the same experiment, using $\alpha_2\delta$-3 as substrate, and observed a similar reduction in its proteolytic cleavage of 53.9%, in the cell surface biotinylated fraction of *ADAM10*$^{-/-}$/*ADAM17*$^{-/-}$ cells compared to CRISPR WT cells (P = .0002, Figure 2D and E).

Next, we examined whether the loss of ADAM10 or ADAM17 was responsible for this effect, by using single knockout cell lines. We found a significant 39.1 ± 3.4% (P < .0001) reduction in proteolytic cleavage of $\alpha_2\delta$-1 in cell surface biotinylated fractions from *ADAM17*$^{-/-}$ compared to control cells, whereas there was a small increase in $\alpha_2\delta$-1 cleavage in *ADAM10*$^{-/-}$ cells (Figure 2F and G).

Effect of ADAM17 or ADAM10 Knockout on Calcium Channel Currents and Cell Surface Expression

We then wished to examine whether the reduction in proteolytic cleavage of $\alpha_2\delta$-1 by ADAM17 had a functional effect on Ca_V currents, as would be predicted from our previous study, in which we showed noncleavable $\alpha_2\delta$ constructs were nonfunctional in this regard.[13] We first examined Ca_V currents formed by $Ca_V2.2$ together with β1b and $\alpha_2\delta$-1, expressed in *ADAM17*$^{-/-}$ or *ADAM10*$^{-/-}$ HEK293 cells, compared to CRISPR WT cells. There was a clear reduction in I_{Ba} (by 44.5% at +5 mV, P = .0002; Figure 3A and B) in *ADAM17*$^{-/-}$ but not *ADAM10*$^{-/-}$ cells, with no change in the potential for half-activation, $V_{50,\,act}$ (Figure 3B).

If the reduction in $Ca_V2.2$-mediated I_{Ba} in *ADAM17*$^{-/-}$ cells relates to the reduced cleavage of $\alpha_2\delta$-1, then it should also occur for another channel subtype. We, therefore, examined $Ca_V1.2$, co-expressing it with $\alpha_2\delta$-1 and a different β (β3), comparing CRISPR WT cells with *ADAM17*$^{-/-}$ cells (Figure 3C and D). We found a reduction in peak I_{Ba} for $Ca_V1.2$ in ADAM17$^{-/-}$ cells (by 53.5% at +20 mV, P < .0001), which was similar to that found for $Ca_V2.2$, thereby implicating $\alpha_2\delta$-1 in this reduction. As for $Ca_V2.2$, there was no significant change in the $V_{50,\,act}$ (Figure 3D).

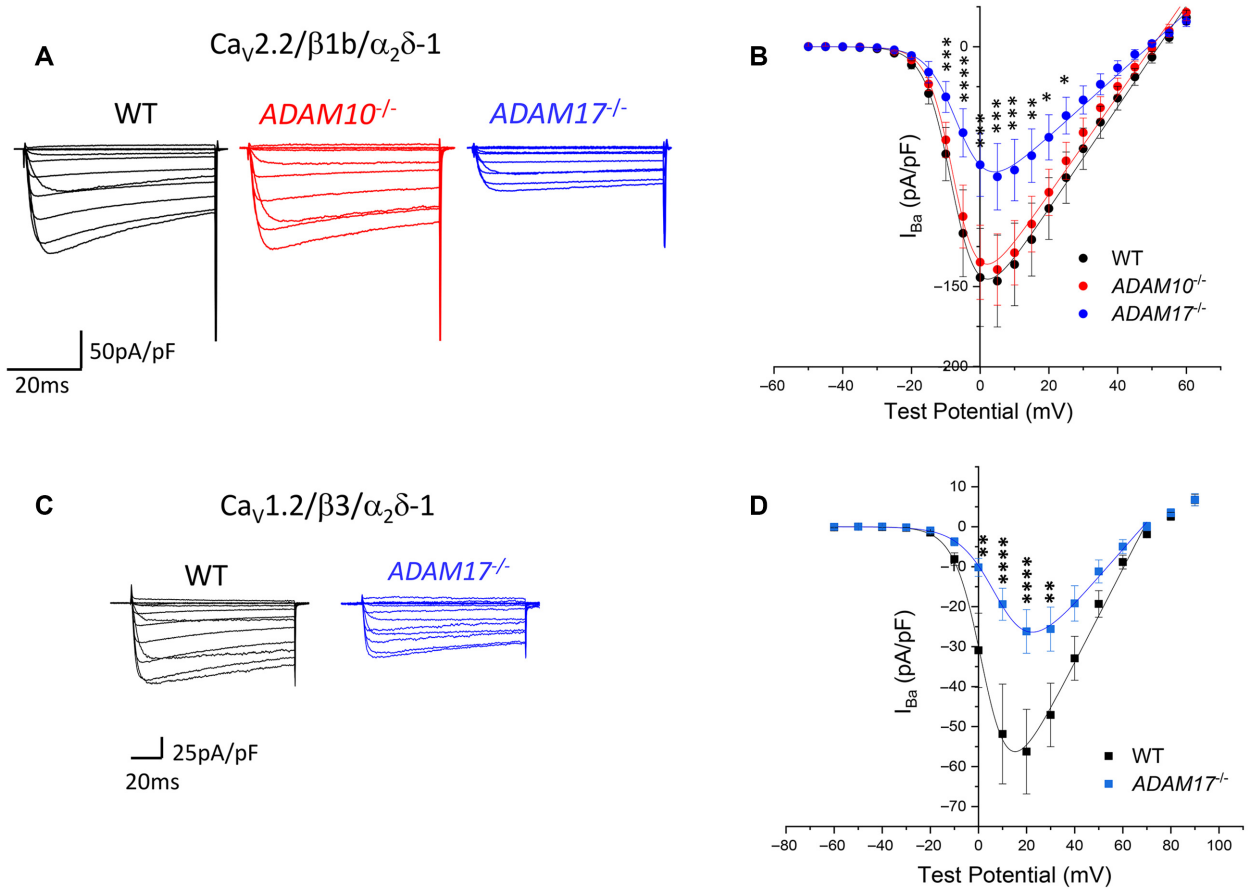

Figure 3. Knockout of *ADAM17*, but not *ADAM10*, decreases $Ca_V2.2$ and $Ca_V1.2$ currents. (A) Examples of I_{Ba} currents for $Ca_V2.2$ expressed in CRISPR WT HEK293 cells (black), *ADAM10*$^{-/-}$ cells (red) and *ADAM17*$^{-/-}$ cells (blue). $Ca_V2.2$ is co-expressed with $\beta1b$ and $\alpha_2\delta$-1. Holding potential −80 mV, steps between −50 mV and +60 mV for 50 ms. (B) Mean (± SEM) current–voltage (*I–V*) relationships for the conditions shown in (A). Control (black; $n = 23$), *ADAM10*$^{-/-}$ (red, $n = 29$), and *ADAM17*$^{-/-}$ (blue; $n = 21$). The individual and mean *I–V* data were fit with a modified Boltzmann equation (see Methods). $V_{50,\,act}$ values are −5.9 ± 1.4 mV (Control), −5.8 ± 0.8 mV (*ADAM10*$^{-/-}$), and −2.5 ± 1.36 mV (*ADAM17*$^{-/-}$). Two-Way ANOVA with Sidak's post hoc test correction for multiple comparisons was performed for the *I–V* data: $^{*}P < .05$, $^{**}P < .01$, $^{***}P < .001$, and $^{****}P < .0001$. (C) Examples of I_{Ba} currents for $Ca_V1.2$ expressed in CRISPR WT HEK293 cells (black) and *ADAM17*$^{-/-}$ cells (blue). $Ca_V1.2$ is co-expressed with $\beta3$ and $\alpha_2\delta$-1. Holding potential −80 mV, steps between −60 and +90 mV for 50 ms. (D) Mean (± SEM) *I–V* relationships for the conditions shown in (C). Control (black; $n = 26$) and *ADAM17*$^{-/-}$ (blue; $n = 19$). The individual and mean *I–V* data were fit with a modified Boltzmann equation as in (B). $V_{50,\,act}$ values are 5.8 ± 1.0 mV (Control) and 6.5 ± 1.9 mV (*ADAM17*$^{-/-}$). Statistical differences between the two sets of *I–V* data were examined at each potential and corrected for multiple *t*-tests with Holm Sidak's post hoc correction: $^{**}P < .01$, $^{****}P < .0001$.

In order to determine whether the effect on Ca_V currents of expression in *ADAM17*$^{-/-}$ cells was related to an effect on trafficking of the channels, we examined the cell surface expression of $Ca_V2.2$ (in the presence of $\beta1b$ and $\alpha_2\delta$-1), using the exofacial HA epitope on a GFP_$Ca_V2.2$-HA construct, relative to its cytoplasmic expression, measured by GFP, as described previously.[15,53] In contrast to the marked reduction in $Ca_V2.2$ currents in *ADAM17*$^{-/-}$ cells, there was no effect on cell surface expression of the channel, as measured by the HA/GFP ratio (Figure 4A and B), indicating that there was no influence of *ADAM17* knockout on $Ca_V2.2$ trafficking. This would agree with our previous finding that $Ca_V2.2$ cell surface expression in non-neuronal cells was still increased by a noncleavable $\alpha_2\delta$-1 construct.[13] This result reinforces our finding that the cleavage of $\alpha_2\delta$-1 is not essential for calcium channel trafficking to the plasma membrane in undifferentiated cell lines, but is essential for enhancing calcium channel function.[13] Of interest, there was a small increase in $Ca_V2.2$ cell surface expression in *ADAM10*$^{-/-}$ cells, relative to the CRISPR WT cells (Figure 4B), and this could relate to the increased proteolytic cleavage of $\alpha_2\delta$-1 in the cell surface fraction of *ADAM10*$^{-/-}$ cells (Figure 2G), since the % cleavage of $\alpha_2\delta$-1 is elevated in cell surface biotinylated fractions.[33]

Subcellular Site of Proteolytic Cleavage

In a previous study, we found that cleaved $\alpha_2\delta$-1 is associated with a mature glycosylation pattern, as N-linked glycans are trimmed and modified in the Golgi apparatus,[54] although some membrane proteins can bypass this route.[55] Conversely, uncleaved $\alpha_2\delta$-1 primarily possesses immature endoplasmic reticulum (ER)-associated glycosylation that can be removed by endoglycosidase-H (Endo-H) in WCL fractions[56] (see diagram in Figure 5A). This suggests that $\alpha_2\delta$ proteolytic cleavage is likely to be associated mainly with post-ER organelles, including the Golgi apparatus.[56] Nevertheless, it is also the case that $\alpha_2\delta$ cleavage can be induced to occur on the plasma membrane.[13]

In order to examine whether $\alpha_2\delta$-1 needs to be trafficked through the Golgi to be proteolytically cleaved by ADAM17 protease, we pursued several experimental routes. First, we used a constitutively active mutant ADP ribosylation factor (Arf)1 (Q71L), which blocks traffic between ER and Golgi,[57] and promotes the utilization of an unconventional endosomal pathway to the cell surface that bypasses the Golgi apparatus.[58] Confirming this alternative trafficking route is available in HEK293 cells,

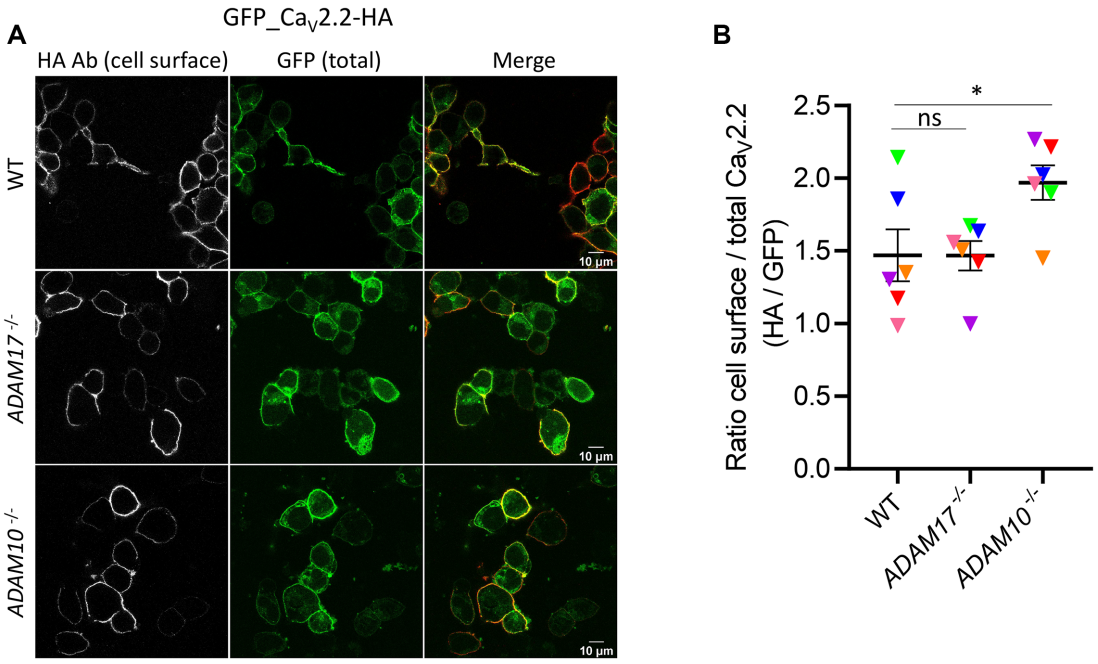

Figure 4. *ADAM17* knockout does not alter the cell surface expression of $Ca_V2.2$ at the plasma membrane. (A) Confocal images of GFP_$Ca_V2.2$-HA expressed in CRISPR WT (top), *ADAM17*$^{-/-}$ (middle) or *ADAM10*$^{-/-}$ (bottom) HEK293 cells. All conditions contained β1b and $\alpha_2\delta$-1. Cell surface staining of GFP_$Ca_V2.2$-HA was obtained by incubating the cells with HA Ab in nonpermeabilized cells (left, white). The total expression of GFP_$Ca_V2.2$-HA is determined by the cytoplasmic GFP signal (middle), the merged images are shown on the right (HA in red). Scale bars, 10 μm. (B) Scatter plot (mean ± SEM with individual data points for six independent transfections, with all conditions in parallel), showing the ratio of cell surface to total $Ca_V2.2$ (HA/GFP) in CRISPR WT, *ADAM17*$^{-/-}$or *ADAM10*$^{-/-}$ HEK293 cells. Each individual data point represents a mean of ratio HA/GFP of ~100 cells/experiment. ns = nonsignificant for WT vs. *ADAM17*$^{-/-}$; *P = .0379 for WT vs. *ADAM10*$^{-/-}$, one-way ANOVA, and Tukey's post hoc test, correcting for multiple comparisons.

we found that, in the presence of Arf1(Q71L), $\alpha_2\delta$-1 was still able to reach the cell surface (Figure 5B).

Under control conditions, $\alpha_2\delta$-1 in the cell surface biotinylated fraction was mainly Endo-H-resistant in both CRISPR WT and *ADAM17*$^{-/-}$ cells, indicating that it had been trafficked to the plasma membrane via the Golgi apparatus, where it had obtained mature N-glycans (Figure 5B, lanes 1 and 3; Figure S2A). By contrast, in the presence of Arf1(Q71L), $\alpha_2\delta$-1 in the cell surface biotinylated fraction was completely Endo-H-sensitive in both CRISPR WT and *ADAM17*$^{-/-}$ HEK293 cells (Figure 5B, lanes 2 and 4; Figure S2A), indicating that, in this case, $\alpha_2\delta$-1 at the plasma membrane contained only immature N-glycans derived from the ER, and that it had not been processed in the Golgi. As expected, in the WCL most $\alpha_2\delta$-1 was Endo-H-sensitive, suggesting it was mainly derived from the ER fraction, as only a small proportion reaches the plasma membrane (Figure S2B).

In agreement with data presented in Figure 2, we observed less proteolytic cleavage of cell surface biotinylated $\alpha_2\delta$-1 to α_2–1 in *ADAM17*$^{-/-}$ compared to WT cells (58.3% reduction, Figure 5C and D). Proteolytic cleavage of cell surface $\alpha_2\delta$-1 was also significantly reduced by Arf1(Q71L) expression in WT cells by 61.9%, and residual cleavage was further reduced in *ADAM17*$^{-/-}$ cells by 73.9% (Figure 5C and D), indicating that the Golgi apparatus is an important site of proteolytic cleavage of $\alpha_2\delta$-1. Interestingly expression of Arf1(Q71L) also promoted the appearance of an intermediate MW species of cleaved $\alpha_2\delta$-1, which may represent cleavage of $\alpha_2\delta$-1 at an alternative site, or an intermediate product (Figure 5C, *).

The conclusion that cleavage of $\alpha_2\delta$ proteins is associated in part with the Golgi apparatus was also borne out by subcellular fractionation of an $\alpha_2\delta$-3 stable SH-SY5Y cell line, in which uncleaved $\alpha_2\delta$-3 is associated with an ER marker, protein disulfide isomerase (PDI), whereas the appearance of cleaved α_2–3 and δ-3 moieties are associated with the presence of the Golgi marker, g97 (Figure S3A and B).

In order to determine whether cleavage of $\alpha_2\delta$ proteins could also occur on the cell surface, we examined the efficacy of the tissue inhibitor of metalloproteases (TIMP-3). TIMPs are endogenously expressed small proteins, secreted in the extracellular matrix, which differentially inhibit particular MMPs and ADAMs,[59] although their actions are complex and may also involve activation of some MMPs via ternary complex formation.[60] TIMP-3 inhibits most MMPs and ADAMs, including ADAM17,[59] whereas the catalytically active N-terminal domain (N-TIMP-3) selectively inhibits ADAM17,[59] but not ADAM10.[61] Thus, for this study we applied N-TIMP-3 protein (100 nM, for 24 h) extracellularly to cells expressing $\alpha_2\delta$-1. As expected, N-TIMP-3 did not inhibit cleavage of $\alpha_2\delta$-1 in the WCL (Figure 6A and B), but it significantly reduced cleavage of cell surface $\alpha_2\delta$-1 (by 21%, P = .023; Figure 6A and C). This result indicates that at least some cleavage of $\alpha_2\delta$-1 can occur at the plasma membrane. This experiment also confirms that ADAM17 is likely to be involved in this process.

Discussion

Cleavage of $\alpha_2\delta$-1 Involves ADAM17

The importance of $\alpha_2\delta$-1 in multiple disorders,[62] and its relevance as a therapeutic target,[28] coupled with our finding that its proteolytic cleavage into mature disulfide-bonded α_2 and δ is required for the enhancement of calcium channel function,[13] suggested to us that targeting the proteolytic cleavage of $\alpha_2\delta$-1 could represent a novel site for therapeutic intervention. The

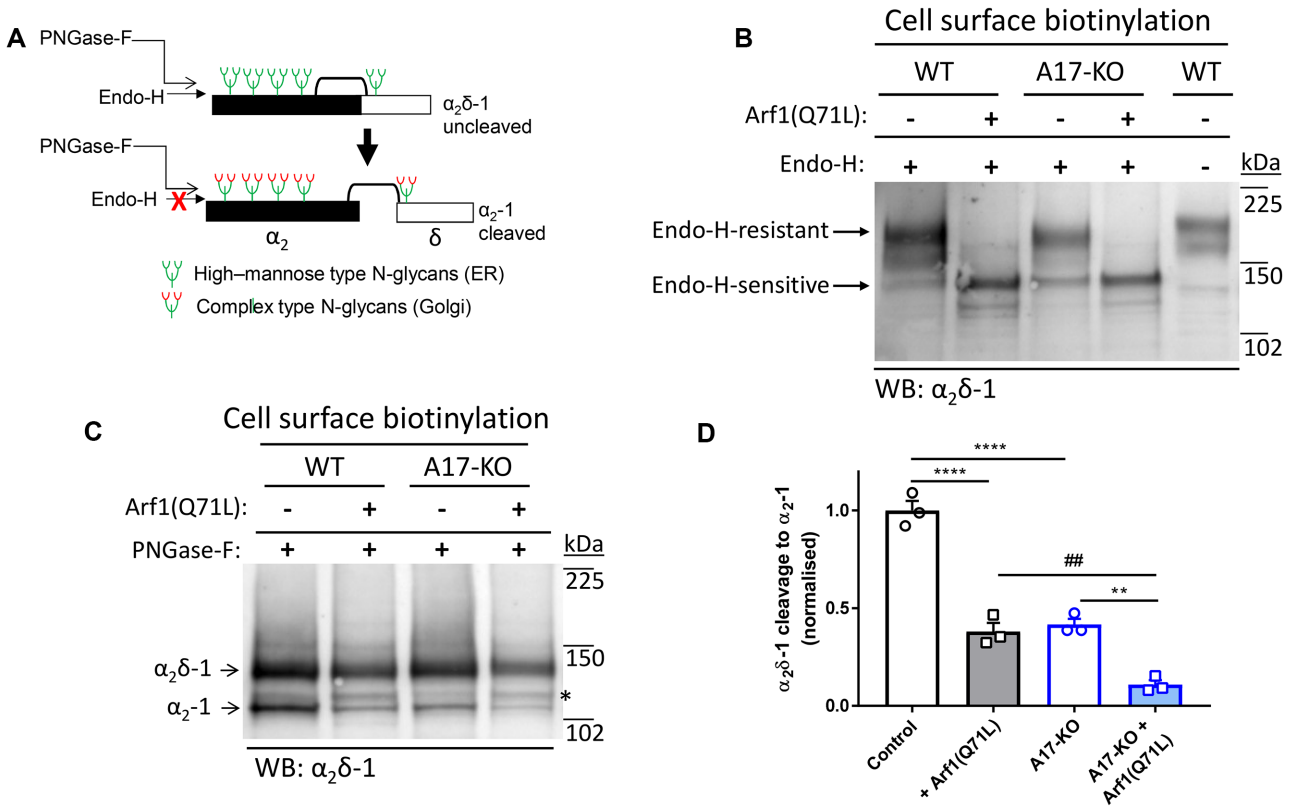

Figure 5. Effect of block of ER–Golgi trafficking and stimulation of alternative route to cell surface by Arf1(Q71L) on cleavage and N-glycosylation pattern of $\alpha_2\delta$-1 in CRISPR WT and *ADAM17*$^{-/-}$ cells. (A) Schematic representation of post-translational modifications of $\alpha_2\delta$-1. Immature glycosylation, occurring in the ER, is sensitive to Endo-H, whereas mature glycosylation, occurring in the Golgi, is resistant to Endo-H. There are differential effects of Endo-H on uncleaved (top) and cleaved (bottom) $\alpha_2\delta$-1. (B) Effect of expression of $\alpha_2\delta$-1 in CRISPR WT (lanes 1, 2, and 5) and *ADAM17*$^{-/-}$ (A17-KO) cells (lanes 3 and 4) in the absence (lanes 1, 3, and 5) and presence (lanes 2 and 4) of the ER-to-Golgi blocker, Arf1(Q71L), in cell surface biotinylated samples, to show fraction at the plasma membrane, either treated with Endo-H (lanes 1–4) or left untreated (lane 5) for comparison. The sizes of the Endo-H-resistant bands (after mature glycosylation in the Golgi) and Endo-H-sensitive bands (after blocking ER-to-Golgi transport using Arf1(Q71L)) are indicated with arrows. Representative of $n = 3$ separate experiments. (C) Effect of expression of $\alpha_2\delta$-1 in CRISPR WT (lanes 1 and 2) and *ADAM17*$^{-/-}$ (A17-KO) cells (lanes 3 and 4) in the absence (lanes 1 and 3) and presence (lanes 2 and 4) of Arf1(Q71L). Samples are biotinylated and fully deglycosylated with PNGase-F to show uncleaved-$\alpha_2\delta$-1 (upper band) and cleaved α_2–1 (lower band). The absolute % cleavage of $\alpha_2\delta$-1 to cleaved α_2–1 was 27.3 ± 1.3% in control CRISPR WT cells ($n = 3$). *indicates an intermediate species, which may represent cleavage of $\alpha_2\delta$-1 at an alternative site, or an intermediate product. (D) Quantification of the effect of of Arf1(Q71L) (shaded compared to open bars) in WT (black bars) and *ADAM17*$^{-/-}$ cells (blue bars) on cleavage of cell surface biotinylated $\alpha_2\delta$-1, normalized to that in control CRISPR WT cells. Data are mean ± SEM and individual data for three separate experiments, including that in (C). Statistical differences determined using one-way ANOVA and Sidak's multiple comparison test; ****$P < .0001$; **$P = .0017$; ## $P = .0037$.

structure of the $\alpha_2\delta$-1 subunit[11] does not completely resolve the proteolytic cleavage site, and the C-terminus of α_2 and N-terminus of δ are not co-located, with some missing sequence. This might indicate that either these termini are dynamic within the structure, and a conformational change might occur on proteolytic cleavage of $\alpha_2\delta$ such that they could move apart, or that a loop of $\alpha_2\delta$-1 might be excised by successive proteolytic cleavages, as occurs for some other proteins.[50]

In this study, we have identified that ADAM17 is a key protease involved in proteolytic processing of pro-$\alpha_2\delta$-1 and $\alpha_2\delta$-3 subunits. We provide three lines of evidence for the role of ADAM17: First, proteolytic cleavage is inhibited by chemical inhibitors of particular MMPs and ADAMs, including ADAM17. Second, proteolytic cleavage of $\alpha_2\delta$-1 and $\alpha_2\delta$-3 is markedly reduced in cell lines by knockout of *ADAM17* but not by knockout of *ADAM10*. Third, proteolytic cleavage of $\alpha_2\delta$-1 is reduced by the N-terminal active domain of TIMP-3 (N-TIMP-3), which selectively inhibits ADAM17. Nevertheless, the incomplete block of cleavage of $\alpha_2\delta$-1 in ADAM17$^{-/-}$ cells indicates other proteases are likely to be involved, either at the same or nearby cleavage sites between α_2 and δ, as also occurs for many other proteins, for example amyloid precursor protein.[63] This is borne out by the observation of an additional higher molecular weight α_2 band observed here. Furthermore, ADAM17 is itself involved in protease cascades, and requires activation by other proteases.[50,64]

The Importance of $\alpha_2\delta$-1 Cleavage for Calcium Channel Function

In heterologous systems, the co-expression of $\alpha_2\delta$ subunits has been shown by many groups to increase the recorded calcium channel currents for Ca_V1 and Ca_V2 channels by 3–10-fold.[17,18,65–69] We found previously that this enhancement requires the proteolytic cleavage of $\alpha_2\delta$ into α_2 and δ, and for $Ca_V2.2$ we further showed, using uncleavable $\alpha_2\delta$ constructs, that this process was independent of the increased cell surface expression of the channel.[13] Thus, the effect of $\alpha_2\delta$-1 and $\alpha_2\delta$-3 on calcium channel trafficking to the plasma membrane in undifferentiated cell lines did not require $\alpha_2\delta$ proteolytic cleavage; nevertheless the $\alpha_2\delta$-mediated potentiation of calcium channel currents requires a molecular switch provided by proteolytic cleavage of the $\alpha_2\delta$ subunit.[13]

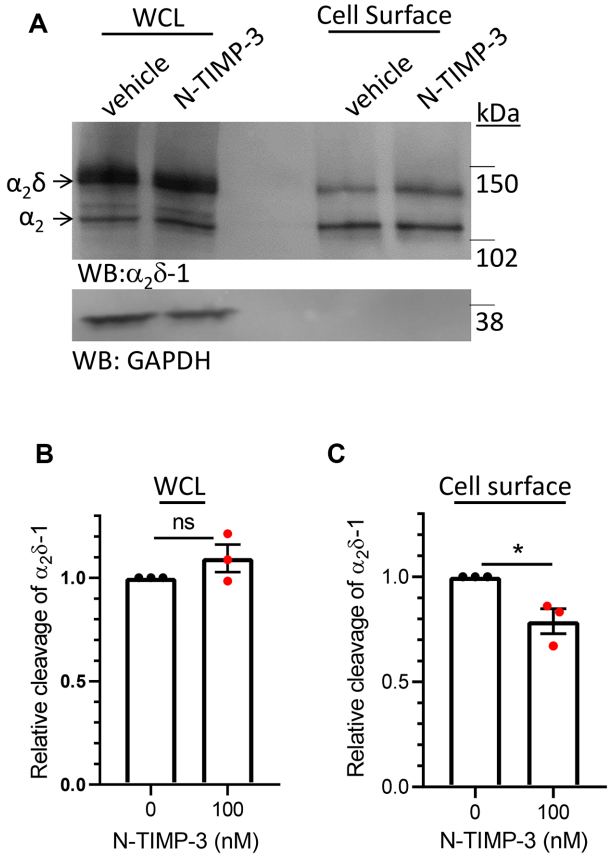

Figure 6. N-TIMP-3 inhibits cleavage of $\alpha_2\delta$-1 on cell surface of tsA-201 cells. (A) Effect of extracellular application of N-TIMP-3 (lanes 2 and 5) compared to control (lanes 1 and 4), on cleavage in WCL (lanes 1 and 2) and cell surface biotinylated fractions (lanes 4 and 5) of HA-$\alpha_2\delta$-1 expressed in tsA-201 cells (upper panel: $\alpha_2\delta$-1 immunoblot), deglycosylated to allow resolution between pro-$\alpha_2\delta$-1 (upper band) and the cleaved form, α_2–1 (lower band). Lower panel, loading and biotinylation control: Endogenous GAPDH. (B) and (C) Quantification of the effect of N-TIMP-3 application on relative cleavage of $\alpha_2\delta$-1 in WCL (B) and at plasma membrane (C) (mean ± SEM and individual data shown for three separate experiments, each normalized to that under control conditions). *$P = .0231$ (Student's *t*-test).

Here, we show that knockout of *ADAM17*, which inhibits $\alpha_2\delta$-1 cleavage, has a clear functional consequence for calcium channel currents, since both $Ca_V2.2$ and $Ca_V1.2$ currents (both in the presence of $\alpha_2\delta$-1, but with different β subunits, β1b and β3, respectively) are significantly reduced by 40%–50% in *ADAM17*$^{-/-}$ cells, compared to either CRISPR WT or *ADAM10*$^{-/-}$ cells. In contrast, and as also predicted from our previous study,[13] there was no effect of *ADAM17* knockout on the $\alpha_2\delta$-1-mediated increase in cell surface expression of $Ca_V2.2$.

Subcellular Site of Proteolytic Processing of $\alpha_2\delta$

In a previous study, we found that native $\alpha_2\delta$-1 was completely processed in axons,[13] despite being intracellular until it reached synaptic terminals.[26] This agrees with our present results indicating that $\alpha_2\delta$ processing begins to occur intracellularly in the Golgi complex, and also with the finding that uncleaved $\alpha_2\delta$, unlike cleaved $\alpha_2\delta$, exhibits an immature glycosylation pattern.[56]

This conclusion is supported by our finding that mutant Arf1(Q71L), which promotes an alternative pathway for $\alpha_2\delta$-1 to reach the cell surface, bypassing the Golgi apparatus,[55] reduces proteolytic cleavage of $\alpha_2\delta$-1, in synergy with *ADAM17* knockout. However, a proportion of $\alpha_2\delta$-1 is still cleaved in the presence of Arf1(Q71L), despite it being completely Endo-H-sensitive, suggesting that the Golgi is not the only site where cleavage can occur, and that mature N-glycosylation is not essential for proteolytic cleavage to occur. Furthermore, the finding that extracellular application of N-TIMP-3 protein produces some inhibition of $\alpha_2\delta$-1 cleavage indicates that cleavage can also occur on the cell surface, although it should be noted that TIMP proteins can also be endocytosed,[70] and thus cleavage of $\alpha_2\delta$-1 could also occur in the endosomal network. The subcellular distribution of ADAM17 would agree with these findings as although most ADAM17 is present intracellularly,[71] and it is activated by furin in the Golgi complex,[72] nevertheless some active ADAM17 is expressed on the cell surface.[71]

Of relevance to our current study, we have recently characterized a single nucleotide mutation in *CACNA2D1*,[73] which results in a substitution of Aspartate for Glycine at position 209, which is in the recently identified double Cache domain (dCache1)[29] of $\alpha_2\delta$-1. This mutation leads to a nonfunctional protein that does not traffic beyond the ER, and is not proteolytically processed into α_2 and δ.[73]

Relevance of $\alpha_2\delta$-1 Function to Pain

There is strong upregulation of $\alpha_2\delta$-1 mRNA and protein in rodent neuropathic injury models.[24–26] Furthermore, overexpression of $\alpha_2\delta$-1 mimics neuropathic allodynia,[74] whereas knockout of $\alpha_2\delta$-1 markedly delays the onset of neuropathic mechanical allodynia.[27] We have shown previously that native pro-$\alpha_2\delta$-1 (presumably newly synthesized) can be observed in the cell bodies of dorsal root ganglion neurons.[13] ADAM17 has many substrates[64] and ADAM17 inhibitors have many potential therapeutic targets.[75] However, *ADAM17* knockout mice are nonviable,[76] which has hampered research into its many functions. Nevertheless, partial knockdown of ADAM17 has been shown to impair mechanical, heat, and cold nociception,[77] although the mechanism for this was not explored. Furthermore, *ADAM17* knockout in specific neurons has been found to reduce excitation.[78]

Conclusion

Proteolytic processing of many proteins, including calcium channels, is involved in their mature function.[79,80] We know from our previous work that proteolytic cleavage into mature $\alpha_2\delta$ is essential for the enhancement of Ca_V function.[13,23] Our present study identifies a key protease involved in proteolytic maturation of $\alpha_2\delta$-1 and $\alpha_2\delta$-3 to be ADAM17, and in agreement with this, knockout of *ADAM17* inhibited the ability of $\alpha_2\delta$-1 to enhance calcium currents. Coupled with our finding that some proteolytic cleavage of $\alpha_2\delta$-1 can occur at the plasma membrane, this opens a potential novel therapeutic target, for example in neuropathic pain.

Contact for Reagents

Further information and requests for resources and reagents should be directed to and will be fulfilled where possible by the Lead Contacts, Annette Dolphin (a.dolphin@ucl.ac.uk) Department of Neuroscience, Physiology and Pharmacology, University College London, Gower Street, London, WC1E 6BT, UK Tel: +44-20–7679 3276 and Ivan Kadurin (i.kadurin@qmul.ac.uk) School

of Biological and Behavioural Sciences, Queen Mary University of London.

Supplementary Material

Supplementary material is available at the *APS Function* online.

Funding

The work of A.C.D. was supported by a Wellcome Trust Investigator award 206279/Z/17/Z, and the work of I.K. was supported in part by the British Heart Foundation grant PG/18/83/34123.

Acknowledgments

We thank Professor Paul Saftig (Biochemisches Institut, Christian-Albrechts-Universität Kiel, Kiel, Germany) for the generous gift of the ADAM17 and ADAM10 knockout and CRISPR WT HEK293 cells, and for very useful advice during the course of this project. We thank Krishma Ramgoolam for her expertise and advice in preliminary experiments.

Authors' Contributions

I.K. performed all the biochemical experiments except those in Figure 5 and Figure S2, performed by K.M.P; S.D. performed all electrophysiology (Figure 3), and imaging (Figure 4); K.M.P. made cDNA constructs; K.C. performed the tissue culture of cell lines and made stable SH-SY5Y cell line; J.I.J.E. performed the initial experiments relating to Figure 2; L.T. and H.N. provided reagents and ideas for the experiments, and reviewed the data; A.C.D. and I.K. conceived the study; and A.C.D., I.K., K.M.P., and S.D. wrote the manuscript aided by all the other authors.

Conflicts of Interest Statement

A.C.D. holds the position of the Editorial Board Member for Function and is blinded from reviewing or making decisions for this manuscript.

Data Availability

The data underlying this article are available in the article and in its online supplementary material.

References

1. Zamponi GW, Striessnig J, Koschak A, Dolphin AC. The physiology, pathology, and pharmacology of voltage-gated calcium channels and their future therapeutic potential. *Pharmacol Rev*. 2015;**67**(4):821–870.
2. Catterall WA. Structure and regulation of voltage-gated Ca^{2+} channels. *Annu Rev Cell Dev Biol*. 2000;**16**(1):521–555.
3. Flockerzi V, Oeken H-J, Hofmann F, Pelzer D, Cavalié A, Trautwein W. Purified dihydropyridine-binding site from skeletal muscle t- tubules is a functional calcium channel. *Nature*. 1986;**323**(6083):66–68.
4. Witcher DR, De Waard M, Sakamoto J, et al. Subunit identification and reconstitution of the N-type Ca^{2+} channel complex purified from brain. *Science*. 1993;**261**(5120):486–489.
5. Takahashi M, Seager MJ, Jones JF, Reber BFX, Catterall WA. Subunit structure of dihydropyridine-sensitive calcium channels from skeletal muscle. *Proc Natl Acad Sci*. 1987;**84**(15):5478–5482.
6. Liu H, De Waard M, Scott VES, Gurnett CA, Lennon VA, Campbell KP. Identification of three subunits of the high affinity w-conotoxin MVIIC-sensitive Ca^{2+} channel. *J Biol Chem*. 1996;**271**(23):13804–13810.
7. Dolphin AC. Calcium channel auxiliary alpha(2)delta and beta subunits: trafficking and one step beyond. *Nat Rev Neurosci*. 2012;**13**(8):542–555.
8. Davies A, Kadurin I, Alvarez-Laviada A, et al. The $\alpha 2\delta$ subunits of voltage-gated calcium channels form GPI-anchored proteins, a post-translational modification essential for function. *Proc Natl Acad Sci*. 2010;**107**(4):1654–1659.
9. Jay SD, Sharp AH, Kahl SD, Vedvick TS, Harpold MM, Campbell KP. Structural characterization of the dihydropyridine-sensitive calcium channel α_2-subunit and the associated δ peptides. *J Biol Chem*. 1991;**266**(5):3287–3293.
10. Ellis SB, Williams ME, Ways NR, et al. Sequence and expression of mRNAs encoding the α_1 and α_2 subunits of a DHP-sensitive calcium channel. *Science*. 1988;**241**(4873):1661–1664.
11. Wu J, Yan Z, Li Z, et al. Structure of the voltage-gated calcium channel Cav1.1 at 3.6 A resolution. *Nature*. 2016;**537**(7619):191–196.
12. Dolphin AC. Voltage-gated calcium channels and their auxiliary subunits: physiology and pathophysiology and pharmacology. *J Physiol*. 2016;**594**(19):5369–5390.
13. Kadurin I, Ferron L, Rothwell SW, et al. Proteolytic maturation of $\alpha 2\delta$ represents a checkpoint for activation and neuronal trafficking of latent calcium channels. *ELife*. 2016;**5**:e21143.
14. Cassidy JS, Ferron L, Kadurin I, Pratt WS, Dolphin AC. Functional exofacially tagged N-type calcium channels elucidate the interaction with auxiliary alpha2delta-1 subunits. *Proc Natl Acad Sci*. 2014;**111**(24):8979–8984.
15. Dahimene S, Page KM, Kadurin I, et al. The alpha2delta-like protein Cachd1 increases N-type calcium currents and cell surface expression and competes with alpha2delta-1. *Cell Rep*. 2018;**25**(6):1610–1621 e1615.
16. Meyer JO, Dolphin AC. Rab11-dependent recycling of calcium channels is mediated by auxiliary subunit alpha2delta-1 but not alpha2delta-3. *Sci Rep*. 2021;**11**(1):10256.
17. Canti C, Nieto-Rostro M, Foucault I, et al. The metal-ion-dependent adhesion site in the Von Willebrand factor-A domain of alpha2delta subunits is key to trafficking voltage-gated Ca2+ channels. *Proc Natl Acad Sci*. 2005;**102**(32):1230–11235.
18. Hendrich J, Tran-Van-Minh A, Heblich F, et al. Pharmacological disruption of calcium channel trafficking by the $\alpha 2\delta$ ligand gabapentin. *Proc Natl Acad Sci*. 2008;**105**(9):3628–3633.
19. Hoppa MB, Lana B, Margas W, Dolphin AC, Ryan TA. alpha2delta expression sets presynaptic calcium channel abundance and release probability. *Nature*. 2012;**486**(7401):122–125.
20. Yurtsever Z, Sala-Rabanal M, Randolph DT, et al. Self-cleavage of human CLCA1 protein by a novel internal metalloprotease domain controls calcium-activated chloride channel activation. *J Biol Chem*. 2012;**287**(50):42138–42149.

21. Placido AI, Pereira CM, Duarte AI, et al. The role of endoplasmic reticulum in amyloid precursor protein processing and trafficking: implications for Alzheimer's disease. *Biochim Biophys Acta*. 2014;**1842**(9):1444–1453.
22. Smith MH, Ploegh HL, Weissman JS. Road to ruin: targeting proteins for degradation in the endoplasmic reticulum. *Science*. 2011;**334**(6059):1086–1090.
23. Ferron L, Kadurin I, Dolphin AC. Proteolytic maturation of alpha2delta controls the probability of synaptic vesicular release. *Elife*. 2018;**7**:e37507. doi: 10.7554/eLife.37507. Last accessed: Jun 19.
24. Newton RA, Bingham S, Case PC, Sanger GJ, Lawson SN. Dorsal root ganglion neurons show increased expression of the calcium channel alpha2delta-1 subunit following partial sciatic nerve injury. *Mol Brain Res*. 2001;**95**(1-2):1–8.
25. Luo ZD, Chaplan SR, Higuera ES, et al. Upregulation of dorsal root ganglion $\alpha_2\delta$ calcium channel subunit and its correlation with allodynia in spinal nerve-injured rats. *J Neurosci*. 2001;**21**(6):1868–1875.
26. Bauer CS, Nieto-Rostro M, Rahman W, et al. The increased trafficking of the calcium channel subunit $\alpha2\delta$-1 to presynaptic terminals in neuropathic pain is inhibited by the $\alpha2\delta$ ligand pregabalin. *J Neurosci*. 2009;**29**(13):4076–4088.
27. Patel R, Bauer CS, Nieto-Rostro M, et al. alpha2delta-1 gene deletion affects somatosensory neuron function and delays mechanical hypersensitivity in response to peripheral nerve damage. *J Neurosci*. 2013;**33**(42):16412–16426.
28. Field MJ, Cox PJ, Stott E, et al. Identification of the $\alpha2\delta$-1 subunit of voltage-dependent calcium channels as a novel molecular target for pain mediating the analgesic actions of pregabalin. *Proc Natl Acad Sci USA*. 2006;**103**(46):17537–17542.
29. Gumerov VM, Andrianova EP, Matilla MA, et al. Amino acid sensor conserved from bacteria to humans. *PNAS*. 2022;**19**(10):e2110415119.
30. Macabuag N, Dolphin AC. Alternative splicing in CaV2.2 regulates neuronal trafficking via adaptor protein complex-1 adaptor protein binding motifs. *J Neurosci*. 2015;**35**(43):14636–14652.
31. Pragnell M, Sakamoto J, Jay SD, Campbell KP. Cloning and tissue-specific expression of the brain calcium channel β-subunit. *FEBS Lett*. 1991;**291**(2):253–258.
32. Kim H-L, Kim H, Lee P, King RG, Chin H. Rat brain expresses an alternatively spliced form of the dihydropyridine-sensitive L-type calcium channel $\alpha2$ subunit. *Proc Natl Acad Sci*. 1992;**89**(8):3251–3255.
33. Kadurin I, Alvarez-Laviada A, Ng SF, et al. Calcium currents are enhanced by alpha2delta-1 lacking its membrane anchor. *J Biol Chem*. 2012;**1287**(40):33554–33566.
34. Shaner NC, Campbell RE, Steinbach PA, Giepmans BN, Palmer AE, Tsien RY. Improved monomeric red, orange and yellow fluorescent proteins derived from *Discosoma* sp. red fluorescent protein. *Nat Biotechnol*. 2004;**22**(12):1567–1572.
35. Cormack BP, Valdivia RH, Falkow S. FACS-optimized mutants of the green fluorescent protein (GFP). *Gene*. 1996;**173**(1):33–38.
36. Presley JF, Ward TH, Pfeifer AC, Siggia ED, Phair RD, Lippincott-Schwartz J. Dissection of COPI and Arf1 dynamics in vivo and role in Golgi membrane transport. *Nature*. 2002;**417**(6885):187–193.
37. Rougier JS, van Bemmelen MX, Bruce MC, et al. Molecular determinants of voltage-gated sodium channel regulation by the Nedd4/Nedd4-like proteins. *Am J Physiol Cell Physiol*. 2005;**288**(3):C692–701.
38. Kashiwagi M, Tortorella M, Nagase H, Brew K. TIMP-3 is a potent inhibitor of aggrecanase 1 (ADAM-TS4) and aggrecanase 2 (ADAM-TS5). *J Biol Chem*. 2001;**276**(16):12501–12504.
39. Riethmueller S, Ehlers JC, Lokau J, et al. Cleavage site localization differentially controls interleukin-6 receptor proteolysis by ADAM10 and ADAM17. *Sci Rep*. 2016;**6**(1):25550. doi: 10.1038/srep25550.
40. Biedler JL, Helson L, Spengler BA. Morphology and growth, tumorigenicity, and cytogenetics of human neuroblastoma cells in continuous culture. *Cancer Res*. 1973;**33**(11):2643–2652.
41. Davies A, Douglas L, Hendrich J, et al. The calcium channel $\alpha2\delta$-2 subunit partitions with CaV2.1 in lipid rafts in cerebellum: implications for localization and function. *J Neurosci*. 2006;**26**(34):8748–8757.
42. Graham JM. Fractionation of Golgi, endoplasmic reticulum, and plasma membrane from cultured cells in a preformed continuous iodixanol gradient. *ScientificWorldJournal* 2002;**2**:1435–1439.
43. Berrow NS, Brice NL, Tedder I, Page K, Dolphin AC. Properties of cloned rat α1A calcium channels transiently expressed in the COS-7 cell line. *Eur J Neurosci*. 1997;**9**(4):739–748.
44. De Jongh KS, Warner C, Catterall WA. Subunits of purified calcium channels. $\alpha2$ and δ are encoded by the same gene. *J Biol Chem*. 1990;**265**(25):14738–14741.
45. Caescu CI, Jeschke GR, Turk BE. Active-site determinants of substrate recognition by the metalloproteinases TACE and ADAM10. *Biochem J*. 2009;**424**(1):79–88.
46. Brou C, Logeat F, Gupta N, et al. A novel proteolytic cleavage involved in Notch signaling: the role of the disintegrin-metalloprotease TACE. *Mol Cell*. 2000;**5**(2):207–216.
47. Grobelny D, Poncz L, Galardy RE. Inhibition of human skin fibroblast collagenase, thermolysin, and *Pseudomonas aeruginosa* elastase by peptide hydroxamic acids. *Biochemistry*. 1992;**31**(31):7152–7154.
48. Solomon A, Rosenblum G, Gonzales PE, et al. Pronounced diversity in electronic and chemical properties between the catalytic zinc sites of tumor necrosis factor-alpha-converting enzyme and matrix metalloproteinases despite their high structural similarity. *J Biol Chem*. 2004;**279**(30):31646–31654.
49. Novak U. ADAM proteins in the brain. *J Clin Neurosci*. 2004;**11**(3):227–235.
50. Wichert R, Scharfenberg F, Colmorgen C, et al. Meprin beta induces activities of A disintegrin and metalloproteinases 9, 10, and 17 by specific prodomain cleavage. *FASEB J*. 2019;**33**(11):11925–11940.
51. Romi E, Gokhman I, Wong E, et al. ADAM metalloproteases promote a developmental switch in responsiveness to the axonal repellant Sema3A. *Nat Commun*. 2014;**5**(1):4058. doi: 10.1038/ncomms5058.
52. Chen CD, Li Y, Chen AK, et al. Identification of the cleavage sites leading to the shed forms of human and mouse anti-aging and cognition-enhancing protein Klotho. *PLoS ONE*. 2020;**15**(1):e0226382.
53. Meyer JO, Dahimene S, Page KM, et al. Disruption of the key Ca^{2+} binding site in the selectivity filter of neuronal voltage-gated calcium channels inhibits channel trafficking. *Cell Rep*. 2019;**29**(1):22–33.e5.
54. Aebi M, Bernasconi R, Clerc S, Molinari M. N-glycan structures: recognition and processing in the ER. *Trends Biochem Sci*. 2010;**35**(2):74–82.

55. Hanus C, Geptin H, Tushev G, et al. Unconventional secretory processing diversifies neuronal ion channel properties. *Elife* 2016;**5**:e20609. doi: 10.7554/eLife.20609. Last accessed: Sep 28.
56. Kadurin I, Rothwell SW, Lana B, Nieto-Rostro M, Dolphin AC. LRP1 influences trafficking of N-type calcium channels via interaction with the auxiliary alpha2delta-1 subunit. *Sci Rep*. 2017;**7**(1):43802. doi: 10.1038/srep43802.
57. Dascher C, Balch WE. Dominant inhibitory mutants of ARF1 block endoplasmic reticulum to Golgi transport and trigger disassembly of the Golgi apparatus. *J Biol Chem*.1994;**269**(2):1437–1448.
58. Gee HY, Noh SH, Tang BL, Kim KH, Lee MG. Rescue of DeltaF508-CFTR trafficking via a GRASP-dependent unconventional secretion pathway. *Cell*. 2011;**146**(5): 746–760.
59. Brew K, Nagase H. The tissue inhibitors of metalloproteinases (TIMPs): an ancient family with structural and functional diversity. *Biochim Biophys Acta*. 2010;**1803**(1):55–71.
60. Zhao H, Bernardo MM, Osenkowski P, et al. Differential inhibition of membrane type 3 (MT3)-matrix metalloproteinase (MMP) and MT1-MMP by tissue inhibitor of metalloproteinase (TIMP)-2 and TIMP-3 rgulates pro-MMP-2 activation. *J Biol Chem*. 2004;**279**(10):8592–8601.
61. Rapti M, Atkinson SJ, Lee MH, Trim A, Moss M, Murphy G. The isolated N-terminal domains of TIMP-1 and TIMP-3 are insufficient for ADAM10 inhibition. *Biochem J*. 2008;**411**(2):433–439.
62. Dolphin AC. The involvement of calcium channel $\alpha 2\delta$ subunits in diseases and as a therapeutic target. *Pathologies of Calcium Channels*, In Norbert W, Alexandra K . eds. Springer. 2014:97–114. doi: 10.1007/978-3-642-40282-1˙5.
63. Eggert S, Thomas C, Kins S, Hermey G. Trafficking in Alzheimer's disease: modulation of APP transport and processing by the transmembrane proteins LRP1, SorLA, SorCS1c, sortilin, and calsyntenin. *Mol Neurobiol*. 2018;**55**(7):5809–5829.
64. Zunke F, Rose-John S. The shedding protease ADAM17: physiology and pathophysiology. *Biochim Biophys Acta Mol Cell Res*. 2017;**1864**(11 Pt B):2059–2070.
65. Mori Y, Friedrich T, Kim M-S, et al. Primary structure and functional expression from complementary DNA of a brain calcium channel. *Nature*. 1991;**350**(6317): 398–402.
66. Klugbauer N, Lacinova L, Marais E, Hobom M, Hofmann F. Molecular diversity of the calcium channel $\alpha 2$-δ subunit. *J Neurosci*. 1999;**19**(2):684–691.
67. Hobom M, Dai S, Marais E, Lacinova L, Hofmann F, Klugbauer N. Neuronal distribution and functional characterization of the calcium channel $\alpha_2\delta$-2 subunit. *Eur J Neurosci*. 2000;**12**(4):1217–1226.
68. Gao B, Sekido Y, Maximov A, et al. Functional properties of a new voltage-dependent calcium channel alpha(2)delta auxiliary subunit gene (CACNA2D2). *J Biol Chem*. 2000;**275**(16):12237–12242.
69. Barclay J, Balaguero N, Mione M, et al. Ducky mouse phenotype of epilepsy and ataxia is associated with mutations in the *Cacna2d2* gene and decreased calcium channel current in cerebellar Purkinje cells. *J Neurosci*. 2001;**21**(16): 6095–6104.
70. Fan D, Kassiri Z. Biology of tissue inhibitor of metalloproteinase 3 (TIMP3), and its therapeutic implications in cardiovascular pathology. *Front Physiol*. 2020;**11**:661. Last access date: 16 June.
71. Lorenzen I, Lokau J, Korpys Y, et al. Control of ADAM17 activity by regulation of its cellular localisation. *Sci Rep*. 2016;**6**(1):35067.
72. Endres K, Anders A, Kojro E, Gilbert S, Fahrenholz F, Postina R. Tumor necrosis factor-alpha converting enzyme is processed by proprotein-convertases to its mature form which is degraded upon phorbol ester stimulation. *Eur J Biochem*. 2003;**270**(11):2386–2393.
73. Dahimene S, von Elsner L, Holling T, et al. Biallelic CACNA2D1 loss-of-function variants cause early-onset developmental epileptic encephalopathy. *Brain*. 2022; https://doi.org/10.1093/brain/awac081, Last access date: 25 March 2022.
74. Li CY, Zhang XL, Matthews EA, et al. Calcium channel alpha(2)delta(1) subunit mediates spinal hyperexcitability in pain modulation. *Pain*. 2006;**125**(1):20–34.
75. Arribas J, Esselens C. ADAM17 as a therapeutic target in multiple diseases. *Curr Pharm Des*. 2009;**15**(20): 2319–2335.
76. Peschon JJ, Slack JL, Reddy P, et al. An essential role for ectodomain shedding in mammalian development. *Science*. 1998;**282**(5392):1281–1284.
77. Quarta S, Mitric M, Kalpachidou T, et al. Impaired mechanical, heat, and cold nociception in a murine model of genetic TACE/ADAM17 knockdown. *FASEB J*. 2019;**33**(3): 4418–4431.
78. Xu J, Molinas AJR, Mukerjee S, et al. Activation of ADAM17 (a disintegrin and metalloprotease 17) on glutamatergic neurons selectively promotes sympathoexcitation. *Hypertension*. 2019;**73**(6):1266–1274.
79. Buonarati OR, Henderson PB, Murphy GG, Horne MC, Hell JW. Proteolytic processing of the L-type Ca (2+) channel alpha 11.2 subunit in neurons. *F1000Res*. 2017;**6**:1166. doi: 10.12688/f1000research.11808.1. Last access date: 25 March 2022.
80. Hulme JT, Yarov-Yarovoy V, Lin TW, Scheuer T, Catterall WA. Autoinhibitory control of the CaV1.2 channel by its proteolytically processed distal C-terminal domain. *J Physiol*. 2006;**576**(Pt 1):87–102.